Bioconjugate Chemistry

Article

pubs.acs.org/bc

Stepwise Orthogonal Click Chemistry toward Fabrication of Paclitaxel/Galactose Functionalized Fluorescent Nanoparticles for HepG2 Cell Targeting and Delivery

Chian-Hui Lai,[†] Tsung-Che Chang,[†] Yung-Jen Chuang,[‡] Der-Lii Tzou,[§] and Chun-Cheng Lin*[,†,∥]

[†]Department of Chemistry and [‡]Department of Medical Science and Institute of Bioinformatics and Structural Biology, National Tsing Hua University, 101 Sec. 2, Kuang Fu Road, Hsinchu 300, Taiwan

[§]Institute of Chemistry and [∥]Genomic Research Center, Academia Sinica, 128 Sec. 2, Academia Road, Nankang, Taipei 115, Taiwan

Supporting Information

ABSTRACT: In this report, we used stepwise orthogonal click chemistry (SOCC) involving strain-promoted azide–alkyne cycloaddition (SPAAC) and microwave-assisted Cu(I)-catalyzed azide–alkyne cycloaddition (CuAAC) to assemble an anticancer drug (paclitaxel, PTX) and a targeting ligand (trivalent galactoside, TGal) on a fluorescent silicon oxide nanoparticle (NP) by using dialkyne linker **8** as a bridge. The fluorescent **NH_2@Cy3SiO_2NP** was fabricated using a competition method to incorporate Cy3 without loss of the original surface amine density on the NPs. The concept of SOCC was first investigated in a solution-phase model study that showed quantitative reaction yield. In the fabrication of **TGal-PTX@Cy3SiO_2NP**, the expensive compound azido-functionalized PTX **12** used in SPAAC can be easily recovered due to the absence of other reagents in the reaction mixture. High loading of the sugar ligand on the NP surface serves a targeting function and also overcomes the low water solubility of PTX. Confocal fluorescence microscopy and cytotoxicity assay showed that **TGal-PTX@Cy3SiO_2NP** was taken up by HepG2 cells and was affected by the microtubule skeleton in these cells and inhibited the proliferation of these cells in a dose-dependent manner. The presence of a fluorescent probe, a targeting ligand, and an anticancer drug on the multifunctional **TGal-PTX@Cy3SiO_2NP** allows for real-time imaging, specific cancer-cell targeting, and the cell-killing effect which is better than free PTX.

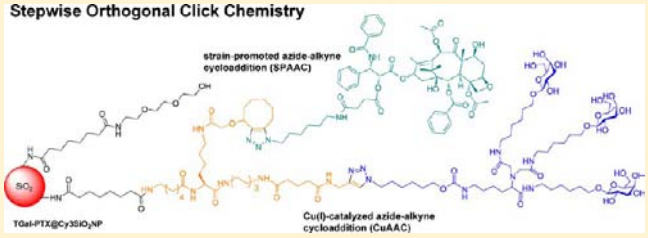

INTRODUCTION

The use of nanoparticle (NP) based therapeutics in cancer treatment has experienced rapidly growing interest in the past years.[1−5] NP surfaces can be engineered so that NPs are effective therapeutic alternatives that overcome previously encountered drawbacks such as nonspecific delivery of antitumor agents, inadequate drug concentrations delivered at the tumor, and multidrug resistance associated with conventional chemotherapeutic agents.[1−5] The high surface-area-to-volume ratio of NPs enables them to be used as multivalent carriers[6−12] to enhance weak ligand–protein interactions and provide high drug concentrations to cancer cells. Abraxane, an albumin-bound paclitaxel NP, was approved by the FDA in 2005 and became the first nanotherapeutic used in 41 countries to treat breast cancer patients for whom combination therapy has failed.[2,3,13] NPs with sizes of 10–100 nm tend to accumulate at the tumor site because of the enhanced permeability and retention (EPR) effect.[14] However, NPs can be rapidly cleared from blood circulation by the reticuloendothelial system (RES), dramatically reducing their *in vivo* therapeutic efficacy. Many efforts have been made to modify the NP surface to enhance its water solubility, half-life, biocompatibility, and target specificity to counteract this effect.[1−3,14]

Due to the ease of synthesis and precise size control,[15,16] the dye-doped silicon oxide NPs have been widely used in a variety of applications[17−19] and were thus chosen as our nanocarrier. The size of silica oxide NP can be controlled by tuning the amount of ammonia in the synthesis process,[20,21] and the size of NP for receptor-mediated endocytosis is also considered to get a longer circulation time.[22,23] Among various dyes available, cyanine dyes are reagents for important clinical and diagnostic applications such as photodynamic therapy, optical recording, and microarrays. Thus, Cy3 was selected to dope in the synthesized silica NP because of its high fluorescence quantum yield and photostability. In this study, to produce a Cy3 fluorescent silicon oxide NP with amino functionality on the surface, a competition method was developed to incorporate Cy3 without losing surface amine density compared to a silicon oxide NP without a fluorescent dye. Besides, the competition method can avoid the drawback of self-quenching caused by tight packing of the dye on NPs.[8,24]

Greater targeting selectivity and better delivery efficiency are desirable in the development of therapeutic agents to enhance

Received: May 7, 2013
Revised: August 27, 2013
Published: August 29, 2013

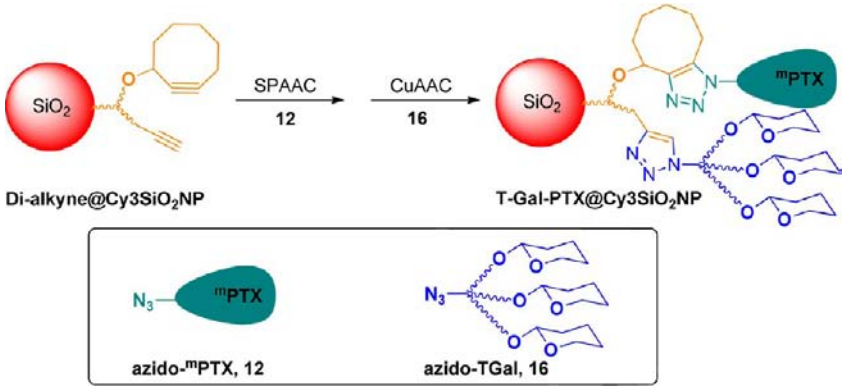

Figure 1. General strategy for stepwise orthogonal click chemistry (SOCC) on fluorescent silicon oxide NPs. The detail chemical structures of **12** and **16** were shown in Scheme 2.

Scheme 1. Synthesis of Di-Alkyne Derivative 8[a]

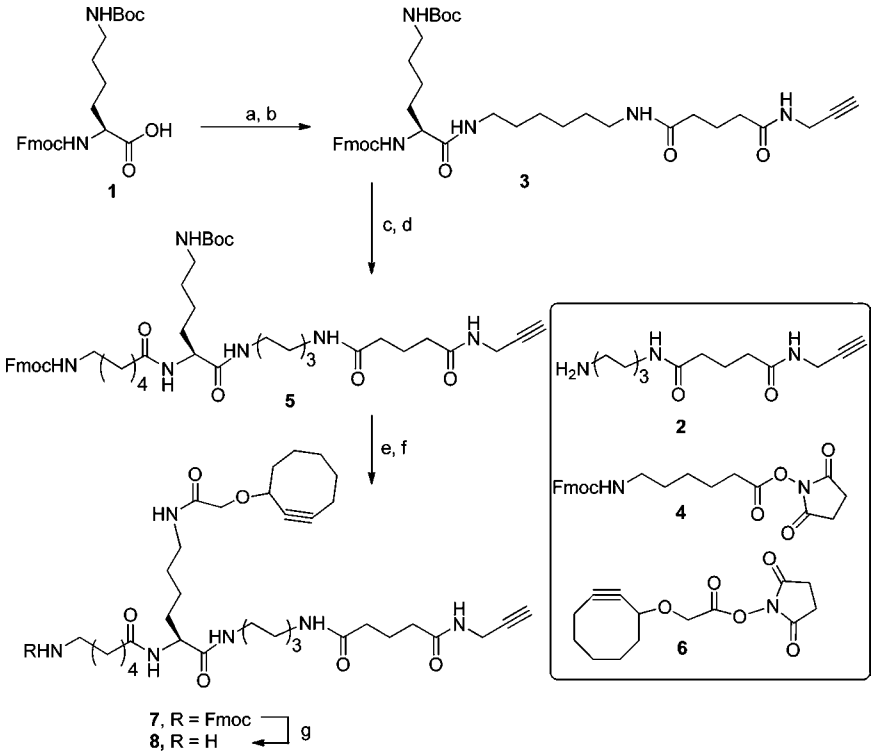

[a]Reagents and conditions: (a) EDC, NHS, DCM, rt, 3 h; (b) **2**, NMM, DCM, 4 °C, 12 h, 72% for two steps; (c) DBU, MeOH, rt, 3 h; (d) **4**, NMM, DMF, 4 °C, 12 h, 75% for two steps; (e) TFA, H_2O, MeOH, rt, 12 h; (f) **6**, NMM, DMF, 4 °C, 18 h; (g) NEt_3, MeOH, rt, 18 h, 62% for three steps.

the intracellular concentration of drugs in tumor cells while avoiding toxicity in normal cells. To achieve this goal, antibody- or ligand-mediated targeting of anticancer therapeutics is currently being explored. The advantage of ligand-targeted therapeutics is that, when NPs bind to specific receptors and enter the cell, they are usually enveloped by endosomes via receptor-mediated endocytosis, bypassing cellular multidrug resistance transporters.[25] An appropriate ligand-decorated multifunctional NP loaded with an anticancer drug can be a precise method for treatment and imaging of cancer due to the combination of the EPR effect and active targeting to a cellular receptor. Previously, we found that adjusting the spatial arrangement of ligands on a magnetic nanoparticle (MNP) to match the distance between carbohydrate binding sites on an asialoglycoprotein receptor (ASPG-R) increased cellular uptake via ASPG-R-mediated endocytosis trigged by multivalent interaction.[8] Furthermore, trivalent galactose was applied on boron neutron capture therapy (BNCT) by conjugating it with carborane to increase the water solubility of the resulting complex and enhance uptake by HepG2.[26] Although PTX-assembled NPs have been reported,[27−36] most examples either are noncovalently linked to PTX or lack targeting ligands on the NPs and have reduced surface availability for PTX loading due to the presence of the targeting ligand. As shown in Figure 1, in continuation of our efforts in the development of nanocarriers for anticancer treatment, we herein report the use of stepwise orthogonal click chemistry (SOCC) to assemble a targeting ligand, triantennary galactose (T-Gal), and an antitumor drug (PTX) on the surface of a fluorescent silicon oxide nanoparticle.

Both the high surface density of the targeting ligand and the high loading of anticancer drug are important factors for the

dx.doi.org/10.1021/bc400219t | Bioconjugate Chem. 2013, 24, 1698−1709

Scheme 2. Synthesis of 12 and 16[a]

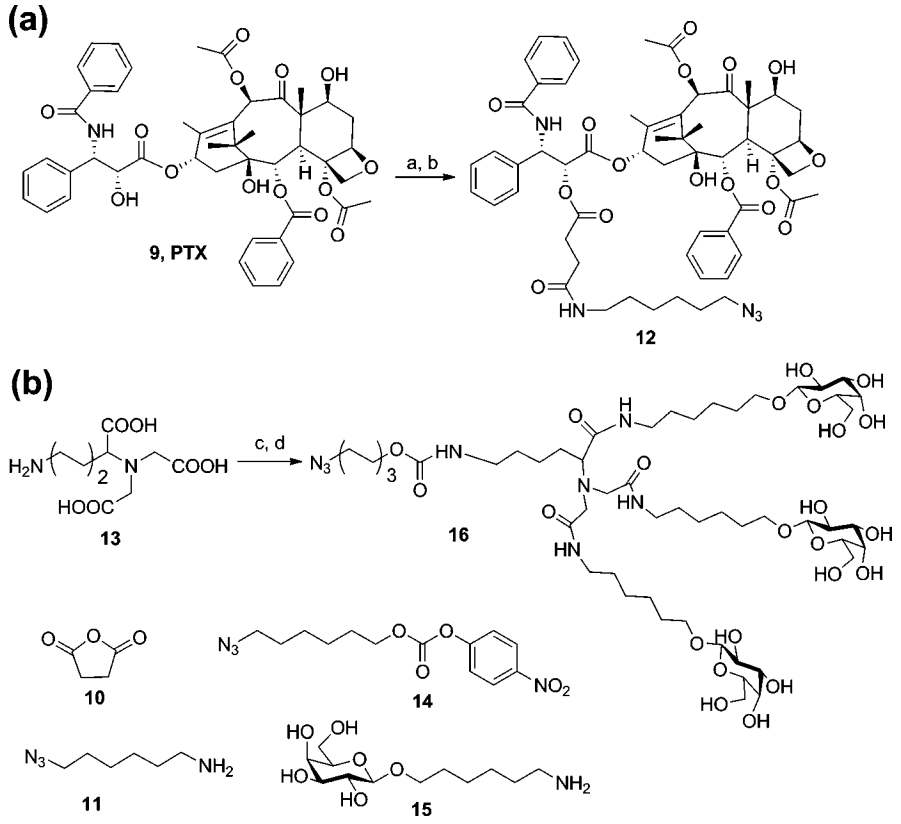

[a]Reagents and conditions: (a) **10**, py., rt, 6 h, 63%; (b) **11**, EDC, HOBt, NEt_3, rt, 18 h, 91%; (c) **14**, NEt_3, DMF, H_2O, rt, 16 h, 88%; (d) **15**, HATU, DMF, NEt_3, 45 °C, 16 h, 47%.

success of a nanocarrier as the anticancer drug. Various research groups[35,37] have designed NPs bearing multifunctional groups by stepwise amide bond formation or controlling the concentrations of reagents used to incorporate these groups on the surface. Apart from conjugation efficiency and precise characterization, after the first reaction in these methods, the surface availability for the incorporation of the second target molecule can be decreased. To achieve highly efficient conjunction of a ligand onto a NP, a SOCC strategy was developed based on the exquisite selectivity and reactivity of alkynes toward azide.[38−40] Although Wolfbeis and co-workers[39,40] have used a peptide with dialkyne as a bridge to cross-link an azido nanoparticle and an azido fluorescent dye for fluorescence resonance energy transfer study, this approach is not suitable to incorporate both ligand and drug on the same particle surface. In this report, we developed a trifunctional linker **8** (Scheme 1) with two alkynes and used SOCC strategy to assemble targeting ligand and anticancer drug on the fluorescent silicon oxide NP.

A dialkyne linker **8** (Scheme 1) with two different alkynes was designed as a prospective precursor to be linked to Cy3-doped silicon oxide NP. First, strain-promoted [3 + 2] azide−alkyne cycloaddition (SPAAC)[41−43] was applied to conjugates with azido PXT **12** (Scheme 2a). Due to no additional reagent being used in this reaction, the expensive azido PXT **12** can be easily recovered. Subsequently, microwave-assisted Cu^I-catalyzed [3 + 2] azide−alkyne cycloaddition (CuAAC) was used to immobilize the T-Gal ligand **16** (Scheme 2b). Our extensive biological studies demonstrate that the synthesized NP can serve as a novel platform for cancer diagnosis and therapy. In addition to serving as the targeting ligand, surface galactose can also enhance the water solubility of PTX, which usually uses Cremophor EL (polyoxyethylated castor oil)/ethanol as a solubilizer; this additive can cause allergic reactions.[44,45]

EXPERIMENTAL PROCEDURES

Materials and Methods. All buffers and solutions were prepared by using Millipore water. The chemicals for the synthesis were all obtained from Sigma-Aldrich. ^1H and ^{13}C NMR spectra were recorded on Bruker AV-400 or DMX-600 MHz. Assignment of ^1H NMR spectra was achieved using 2D methods (COSY). Chemical shifts are expressed in ppm using residual $CDCl_3$ (7.24 ppm) or CD_3OD (3.31 ppm) or D_2O (4.67 ppm at 298 k) as internal standard. Low-resolution and high-resolution mass spectra were recorded under ESI-TOF mass spectra conditions. Analytical thin-layer chromatography (TLC) was performed on precoated plates (Silica Gel 60). Silica gel 60 (E. Merck) was employed for all flash chromatography. All reactions were carried out in oven-dried glassware (120 °C) under an atmosphere of argon unless indicated otherwise. All solvents were dried and distilled by standard techniques.

{5-(9*H*-Fluoren-9-ylmethoxycarbonylamino)-5-[6-(4-prop-2-ynylcarbamoyl-butyrylamino)hexyl carbamoyl]-pentyl}-carbamic acid *tert*-butyl ester (3). A solution of compound **1** (500 mg, 1.07 mmol), EDC (245 mg, 1.28 mmol), and NHS (145 mg, 1.28 mmol) in anhydrous CH_2Cl_2 (20 mL) was stirred at rt for 3 h under N_2. After completion of the reaction as indicated by TLC, the reaction was washed with water and brine twice. The organic layer was dried ($MgSO_4$)

dx.doi.org/10.1021/bc400219t | *Bioconjugate Chem.* 2013, 24, 1698−1709

and concentrated to give an *N*-hydroxysuccinimide derivative. A solution of compound **2** (200 mg, 0.75 mmol) (8 mL), *N*-methyl-morpholine (82 μL, 0.75 mmol), and the *N*-hydroxysuccinimide derivative in anhydrous DMF was stirred at 4 °C for 12 h. After completion of the reaction as indicated by TLC, the solvent was evaporated. The crude mixture was purified by column chromatography on silica gel (EA/Hexane/MeOH, 1/1/0 to 10/10/1, and then CH_2Cl_2/MeOH, 10/1 to 5/1) to give compound **3** (388 mg, 72% yield for two steps). R_f 0.38 (MeOH/CH_2Cl_2, 1/9); ^{1}H NMR (400 MHz, MeOD and $CDCl_3$, δ): 1.30 (6H, m), 1.41 (9H, s), 1.46 (6H, m), 1.62 (1H, m), 1.73 (1H, m), 1.87 (2H, m), 2.18 (4H, td, J = 7.8, 7.8 Hz), 2.44 (1H, t, J = 2.2 Hz), 3.02 (2H, t, J = 6.4 Hz), 3.12 (2H, m), 3.16 (2H, m), 3.92 (2H, d, J = 2.2 Hz), 4.01 (1H, t, 5.4 Hz), 4.19 (1H, t, J = 6.6 Hz), 4.36 (2H, m), 7.29 (2H, t, J = 7.4 Hz), 7.37 (2H, t, J = 7.4 Hz), 7.61 (2H, d, J = 7.4 Hz), 7.75 (2H, d, J = 7.4 Hz); ^{13}C NMR (100 MHz, MeOD and $CDCl_3$, δ): 21.19, 22.13, 24.38, 25.47, 25.52, 27.18, 27.71, 28.26, 28.53, 31.20, 34.07, 34.38, 38.34, 38.47, 39.13, 46.42, 54.46, 65.99, 70.25, 78.13, 78.61, 119.05, 124.20, 126.24, 126.89, 140.57, 143.06, 156.24, 156.42, 172.54, 172.92, 173.17; HRMS (ESI) calcd for $C_{40}H_{55}N_5O_7Na$ $[M + Na]^+$ 740.3999, found 740.3990.

{5-[6-(9*H*-Fluoren-9-ylmethoxycarbonylamino)-hexanoyl amino]-5-[6-(4-prop-2-ynylcarbamoyl-butyrylamino)-hexyl-carbamoyl]-pentyl}-carbamic acid *tert*-butyl ester (5). A solution of compound **3** (360 mg, 0.50 mmol) and 8-diazabicyclo[5.4.0]undec-7-ene (150 μL, 1.01 mmol) in MeOH (20 mL) was stirred at rt for 3 h. After completion of the reaction as indicated by TLC, the solvent was evaporated (R_f 0.14, MeOH/CH_2Cl_2, 1/9). The crude mixture was purified by column chromatography on silica gel (CH_2Cl_2/MeOH, 100/8 to 10/3). The above compound was dissolved in anhydrous DMF (4 mL), and NMM (200 μL, 0.75 mmol) and *N*-hydroxysuccinimide-derived compound **4**[46] were added. The resulting mixture was stirred at 4 °C for 12 h. After completion of the reaction as indicated by TLC, the solvent was evaporated. The crude mixture was purified by column chromatography (CH_2Cl_2/MeOH, 100/1 to 10/1) on silica gel to give compound **5** (305 mg, 75% yield for two steps). R_f 0.29 (MeOH/CH_2Cl_2, 1/9); ^{1}H NMR (400 MHz, MeOD, δ): 1.33 (8H, m), 1.42 (9H, s), 1.48 (8H, m), 1.63 (3H, m), 1.74 (1H, m), 1.88 (2H, dt, J = 7.7, 15.0 Hz), 2.21 (6H, m), 2.58 (1H, t, J = 2.5 Hz), 3.01 (2H, t, J = 6.8 Hz), 3.13 (6H, m), 3.93 (2H, d, J = 2.5 Hz), 4.21 (2H, m), 4.33 (2H, d, J = 6.9 Hz), 7.31 (2H, t, J = 7.4 Hz), 7.39 (2H, t, J = 7.4 Hz), 7.64 (2H, d, J = 7.4 Hz), 7.79 (2H, d, J = 7.4 Hz); ^{13}C NMR (100 MHz, MeOD, δ): 23.15, 24.27, 26.56, 27.39, 27.47, 27.54, 28.81, 29.40, 30.26, 30.57, 32.91, 35.93, 36.24, 36.69, 40.23, 41.10, 41.59, 54.80, 67.57, 72.15, 79.86, 80.65, 120.93, 126.18, 128.15, 128.78, 142.62, 145.36, 158.56, 158.90, 174.39, 174.93, 175.22, 176.09; HRMS (ESI) calcd for $C_{46}H_{66}N_6O_8Na$ $[M + Na]^+$ 853.4840, found 853.4845.

Pentanedioic acid (6-{2-(6-amino-hexanoylamino)-6-[2-(cyclooct-2-ynyloxy)-acetylamino]-hexanoylamino}-hexyl)-amide prop-2-ynylamide (8). Compound **5** (300 mg, 0.36 mmol) was dissolved in a mixture of trifluoroacetic acid (1 mL), water (9 mL), and MeOH (3 mL) at room temperature. After being stirred for 12 h, the solvent was removed under vacuum and then neutralized with Dowex 550A (OH^--form) in MeOH (R_f 0.29, MeOH/CH_2Cl_2, 1/4). After removal of the solvent, the residue was dissolved in anhydrous DMF (4 mL) and NMM (200 μL, 0.75 mmol) and then *N*-hydroxysuccinimide ester **6**[42] (125 mg, 0.45 mmol) was added. The resulting mixture was stirred at 4 °C for 18 h. After completion of the reaction as indicated by TLC, the solvent was evaporated (R_f 0.39, MeOH/CH_2Cl_2, 1/9). The crude mixture was purified by column chromatography on silica gel (CH_2Cl_2/MeOH, 100/2 to 10/2). The above compound was dissolved in a mixture of NEt_3 (5 mL) and MeOH (5 mL) at room temperature. The resulting solution was stirred under N_2 for 18 h. After completion of the reaction as indicated by TLC, the solvent was evaporated. The crude mixture was purified by column chromatography on reverse-phase silica gel (MeOH/H_2O, 1/3 to 1/1) to yield compound **8** (150 mg, 62% yield for three steps). R_f 0.08 (MeOH/H_2O, 10/1, reverse-phase TLC); ^{1}H NMR (400 MHz, MeOD, δ): 1.35 (9H, m), 1.50 (8H, m), 1.66 (8H, m), 1.88 (4H, m), 2.25 (9H, m), 2.59 (1H, s), 2.93 (2H, t, J = 7.3 Hz), 3.18 (8H, m), 3.85 (1H, d, J = 14.9 Hz), 3.94 (2H, d, J = 2.2 Hz), 3.98 (1H, d, J = 14.9 Hz), 4.23 (1H, m), 4.29 (1H, m); ^{13}C NMR (100 MHz, MeOD, δ): 21.21, 23.16, 24.29, 26.12, 26.83, 27.47, 27.54, 28.23, 29.39, 30.17, 30.24, 30.31, 30.84, 32.81, 35.42, 35.93, 36.25, 39.59, 40.22, 40.54, 43.15, 54.85, 69.02, 72.16, 74.29, 80.65, 92.40, 102.36, 172.38, 174.42, 174.94, 175.24, 175.82; HRMS (ESI) calcd for $C_{36}H_{61}N_6O_6$ $[M + H]^+$ 673.4653, found 673.4662.

*Azidopaclitaxel (**12**).* The synthesis of compound **12** was achieved by modifying previously published procedures.[47] Succinic anhydride **10** (0.82 g, 7.21 mmol) was added to a solution of paclitaxel **9** (PTX, 200 mg, 0.23 mmol) in pyridine (3 mL). The resulting mixture was stirred at rt for 6 h. After completion of the reaction as indicated by TLC, the solvent was evaporated (R_f 0.22, EA/Hexane/MeOH, 10/10/1). The residue was suspended in 8 mL of distilled water and stirred for 30 min, followed by centrifugation. The resulting residue was redissolved in acetone, and water was added to precipitate a white solid. The solid was collected by filtration to give the desired product in a 63% yield. Next, the above product (50 mg, 52 μmol), compound **11**,[48] EDC (20 mg, 79 μmol), HOBT(14 mg, 105 μmol), and NEt_3 (10 μL, 105 μmol) were dissolved in anhydrous CH_2Cl_2 (3 mL) at room temperature. The reaction mixture was stirred at rt for 18 h. After completion of the reaction as indicated by TLC, the solvent was evaporated. The crude mixture was purified by column chromatography on silica gel (EA/Hexane/MeOH, 1/1/0 to 10/10/0.8) to give **12** (50 mg, 91% yield). R_f 0.41 (EA/Hexane/MeOH, 10/10/1); ^{1}H NMR (600 MHz, $CDCl_3$, δ): 1.10 (3H, s), 1.19 (3H, s), 1.22 (2H, m), 1.31 (2H, m), 1.41 (2H, dt, J = 7.3, 14.8 Hz), 1.53 (2H, dt, J = 7.0, 14.2 Hz), 1.64 (3H, s), 1.88 (3H, s), 2.06 (2H, m), 2.18 (3H, s), 2.39 (3H, s), 2.41 (2H, m), 2.50 (2H, m), 2.59 (1H, s), 2.71 (2H, t, J = 6.8 Hz), 3.10 (2H, m), 3.21 (2H, t, J = 7.0 Hz), 3.75 (1H, d, J = 7.0 Hz), 4.16 (1H, d, J = 8.5 Hz), 4.27 (1H, d, J = 8.5 Hz), 4.39 (1H, br), 4.93 (1H, d, J = 9.7 Hz), 5.41 (1H, d, J = 4.0 Hz), 5.63 (1H, d, J = 7.0 Hz), 5.71 (1H, t, J = 6.0 Hz), 5.88 (1H, dd, J = 4.0, 8.8 Hz), 6.15 (1H, t, J = 8.3 Hz), 6.26 (1H, s), 7.28 (1H, m), 7.32 (1H, d, J = 8.8 Hz), 7.36 (6H, m), 7.46 (1H, t, J = 7.4 Hz), 7.49 (2H, t, J = 7.7 Hz), 7.59 (1H, t, J = 7.4 Hz), 7.77 (2H, d, J = 7.2 Hz), 8.09 (2H, d, J = 7.2 Hz); ^{13}C NMR (150 MHz, $CDCl_3$, δ): 9.54, 14.69, 20.75, 22.03, 22.57, 26.26, 26.68, 28.60, 29.28, 29.35, 29.61, 30.78, 35.39, 35.49, 39.45, 43.09, 45.53, 51.21, 53.12, 58.37, 71.74, 71.98, 74.30, 75.01, 75.53, 77.20, 78.91, 80.93, 84.36, 126.69, 127.25, 128.43, 128.52, 128.64, 128.97, 129.17, 130.13, 131.85, 132.72, 133.58, 133.61, 137.00, 142.59, 166.86, 167.29, 168.11, 169.80, 170.87, 171.14, 171.83, 203.75; HRMS (ESI) calcd for $C_{57}H_{67}N_5O_{16}Na$ $[M + Na]^+$ 1100.4481, found 1100.4482.

6-Azidohexyl {5-(bis-{[6-(β-D-galactopyranosyl)-hexylcarbamoyl]-methyl}-amino)-5-[6-(β-D-galactopyranosyl)-hexylcarbamoyl]-pentyl}-carbamate (16). A solution of compound **13** (*N*,*N*-bis[carboxymethyl]-L-lysine,[49] 300 mg, 1.15 mmol) and compound **14**[26] (424 mg, 1.37 mmol) in 6 mL anhydrous DMF/H_2O (3/1) was mixed with NEt_3 (399 μL, 2.88 mmol) and then was stirred for 16 h under N_2. After completion of the reaction as indicated by TLC, the solvent was evaporated. The crude mixture was purified by column chromatography on silica gel (MeOH/DCM, 3/100 to 1/1) to give the desired product (437 mg, 88.5%). R_f 0.17 (MeOH/CH_2Cl_2, 1/2). The above (150 mg, 0.24 mmol) was dissolved in anhydrous DMF (3 mL), and then compound **15**[8] (265 mg, 0.95 mmol), HATU (360 mg, 0.95 mmol), and NEt_3 (131 μL, 0.95 mmol) were added under nitrogen. The reaction was stirred at 45 °C for 16 h. After completion of the reaction as indicated by TLC, the solvent was evaporated. The resulting residue was subjected to P2 gel filtration (eluent: H_2O) to remove salt, and the resulting residue was purified using reverse-phase silica gel column chromatography (CH_3CN/H_2O, 1/30 to1/2) to give **16** (134 mg, 46.4% yield). R_f 0.5 (MeCN/H_2O, 1/2, reverse-phase TLC); ^{1}H NMR (400 MHz, MeOD, δ): 1.37 (18H, m), 1.50 (8H, m), 1.59 (12H, m), 3.04 (2H, m), 3.19 (10H, m), 3.37−3.58 (15H, m), 3.70 (6H, m), 3.80 (3H, m), 3.86 (3H, m), 3.98 (2H, t, *J* = 6.2 Hz), 4.18 (3H, d, *J* = 7.0 Hz); ^{13}C NMR (100 MHz, MeOD, δ): 24.80, 26.50 × 3, 26.72, 27.42, 27.77 × 3, 29.76, 30.04, 30.30 × 3, 30.66 × 3, 40.11, 40.26, 41.40, 52.31, 57.07, 62.41 × 3, 65.61 × 2, 67.13, 70.21 × 3, 70.61 × 3, 72.52 × 3, 74.97 × 3, 76.49 × 3, 104.89 × 3, 159.15, 173.74 × 2, 174.57; IR (KBr): 2100 (N_3), 1650 (C═O) cm^{-1}; HRMS (ESI) calcd for $C_{53}H_{98}N_8O_{23}Na$ $[M + Na]^+$ 1237.6643, found 1237.6648.

Synthesis of Compound 17. Compound **7** (10 mg, 11.18 μmol) and compound **12** (12 mg, 11.18 μmol) were dissolved in 3 mL of DMF. The reaction mixture was stirred at rt for 6 h and monitored by TLC. Upon completion of the reaction, the solvent was removed under reduced pressure and the crude product was purified by column chromatography on silica gel (CH_2Cl_2/MeOH, 60/1 to 10/1) to give the desired product (22 mg, quant). R_f 0.39 (CH_2Cl_2/MeOH, 9/1); ^{1}H NMR (600 MHz, $CDCl_3$, δ): 1.10−1.70 (31H, m), 1.71−2.50 (43H, m), 2.80−3.40 (12H, m), 3.74 (1H, d, *J* = 5.8 Hz), 3.97 (2H, m), 4.16 (3H, m), 4.26−4.45 (7H, m), 4.93 (1H, s), 5.28 (1H, s), 5.42 (1H, s), 5.64 (1H, d, *J* = 6.7 Hz), 5.86 (1H, s), 6.11 (1H, s), 6.28 (1H, s), 7.25−7.48 (12H, m), 7.50 (3H, m), 7.57 (3H, m), 7.73 (2H, d, *J* = 6.7 Hz), 7.82 (2H, m), 8.10 (2H, d, *J* = 6.2 Hz); HRMS (ESI) calcd for $C_{108}H_{137}N_{11}O_{24}Na$ $[M + Na]^+$ 1994.9736, found 1994.9751.

Synthesis of Compound 18. Sodium ascorbate (100 μL of a 0.3 M solution in H_2O) and $CuSO_4$ (200 μL in a 30 mM solution in H_2O) were added to a solution of compound **17** (5.4 mg, 2.74 μmol) and compound **16** (3.7 mg, 3.01 μmol) in DMF, H_2O, and THF (1/1/5, 20 mL) under N_2. The mixture was irradiated at 100 W at 75 °C for 30 min, and the reaction was monitored by reverse-phase TLC. After completion of the reaction, the solvent was removed under reduced pressure and the crude product was purified by reverse-phase silica gel column chromatography (CH_3CN/H_2O, gradient from 1/10 to 1/1) to give **18** (8.7 mg, quant). R_f 0.34 (MeCN/H_2O, 1/1, reverse-phase TLC); ^{1}H NMR (600 MHz, MeOD, δ): 1.20−1.70 (57H, m), 1.71−2.61 (55H, m), 3.13−3.28 (24H, m), 3.42−3.56 (15H, m), 3.69−3.85 (7H, m), 3.86−4.02 (8H, m), 4.10−4.42 (15H, m), 4.98 (1H, d, *J* = 8.4 Hz), 5.44 (1H, d, *J* = 6.6 Hz), 5.64 (1H, d, *J* = 7.2 Hz), 5.79 (1H, d, *J* = 6.7 Hz), 6.05 (1H, t, *J* = 9.2 Hz), 6.45 (1H, s), 7.26 (1H, t, *J* = 7.0 Hz), 7.30 (2H, m), 7.38 (2H, m), 7.46 (4H, m), 7.49 (3H, m), 7.50−7.70 (6H, m), 7.79 (2H, d, *J* = 7.4 Hz), 7.83 (2H, d, *J* = 7.9 Hz), 8.11 (2H, d, *J* = 7.1 Hz); HRMS (MALDI) calcd for $C_{161}H_{235}N_{19}O_{47}Na$ $[M + Na]^+$ 3213.7515, found 3213.7595.

HO@SiO$_2$NP. **HO@SiO$_2$NP** was synthesized according to previous reports.[20,21] Particle size can be controlled by the concentration of ammonia (NH_4OH) in the reaction solution; a lower concentration yields smaller nanoparticles. As shown in Scheme 4, tetraethylorthosilicate (TEOS, 1 mL) was stirred with ethanol (10 mL), dd-H_2O (1 mL), and NH_4OH (0.1 mL) at room temperature for 12 h. After washing with propanol (PrOH) three times, 40-nm **HO@SiO$_2$NP** nanoparticles were obtained (200 mg). The nanoparticle **HO@SiO$_2$NP** (50 mg) surface was transformed to an amino functionality using a sol−gel process with 3-amino-propyl trimethoxysilane (APS) to give 50 nm **NH$_2$@SiO$_2$NP** (60 mg).

NH$_2$@Cy3SiO$_2$NP. A chemical competition reaction was used to fabricate the fluorescent **NH$_2$@Cy3SiO$_2$NP** nanoparticles. An alkaline PrOH (15.12 mL) solution of **HO@SiO$_2$NP** (252 mg) was mixed with **Cy3-Si(OMe)$_3$**[50] (5.04 mg), APS (504 mg), dd-H_2O (1.51 mL), and NH_4OH (2.06 mL). The resulting solution was stirred at 55 °C for 15 h to yield 50 nm **NH$_2$@Cy3SiO$_2$NP** which size is similar to **NH$_2$@SiO$_2$NP** (260 mg).

Dialkyne@Cy3SiO$_2$NP. **NH$_2$@Cy3SiO$_2$NP** (10 mg) was suspended in DMSO (0.5 mL), and suberic acid bis-*N*-hydroxysuccinimide ester (DSS, 20 mg, 54.3 μmol), EDC (10 mg, 52.2 μmol), and HOBT (7 mg, 52.2 μmol) were added. The resulting mixture was sonicated at room temperature for 30 min and stirred at rt for another 3 h to give *N*-hydroxysuccinimide (OSu)-activated **@Cy3SiO$_2$NP**. The OSu-activated **@Cy3SiO$_2$NP** was washed with DMSO (1 mL × 3), centrifuged at 13 400 rpm for 20 min, and incubated with compound **8** (10 mg, 14.9 μmol, 30 mM), EDC (10 mg, 52.2 μmol), HOBT (7 mg, 52.2 μmol), and NEt_3 (10 μL) μmol in DMSO at rt for 18 h. The resulting **Dialkyne@Cy3SiO$_2$NP** was washed with DMSO (1 mL), and the remaining activated OSu esters on **Dialkyne@Cy3SiO$_2$NP** were capped with 50 mM amino-triethylene glycol in DMSO (1 mL) at rt for 3 h. The particles were washed with DMF (1 mL) three times, followed by centrifugation at 13 400 rpm for 20 min to give 10 mg of **Dialkyne@Cy3SiO$_2$NP**.

tAlkyne-PTX@Cy3SiO$_2$NP. A solution of **Dialkyne@Cy3SiO$_2$NP** (20 mg) in anhydrous DMF (0.5 mL) and compound **12** (0.5 mL of a 20 mM solution in anhydrous DMF) were stirred at rt for 24 h. After completion of the reaction, the **tAlkyne-PTX@Cy3SiO$_2$NP** was collected by centrifugation at 13 400 rpm for 20 min, and the nanoparticles were washed with DMF (1 mL) three times to give **tAlkyne-PTX@Cy3SiO$_2$NP** (18 mg).

TGal-PTX@Cy3SiO$_2$NP. Sodium ascorbate (100 μL of a 0.3 M solution in H_2O) and $CuSO_4$ (200 μL of a 30 mM solution in H_2O) were added to a solution of **tAlkyne-PTX@Cy3SiO$_2$NP** (6 mg) and compound **16** (10 mg, 8.2 μmol) in a mixture of DMF, H_2O, and THF (1/1/5, 20 mL) under N_2. The mixture was irradiated at 100 W at 75 °C for 60 min. The nanoparticles were washed with DMF (1 mL) three times, 50 mM for EDTA (1 mL) twice, and dd-H_2O (1 mL) three times followed by centrifugation at 13 400 rpm for 20 min to give **TGal-PTX@Cy3SiO$_2$NP** (6 mg).

TGal@Cy3SiO$_2$NP. The **OSu-activated@Cy3SiO$_2$NP** (10 mg) was incubated with trigalactose ligand, **19**[8] (10 mg, 9.6 μmol), EDC (10 mg, 52.2 μmol), HOBT (7 mg, 52.2 μmol), and NEt_3 (10 μL) in 1 mL DMSO (Scheme 4). The mixture was sonicated for 30 min and stirred at rt for 18 h. The resulting **TGal@Cy3SiO$_2$NP** was isolated by centrifugation, and the resulting nanoparticles were washed with DMF three times and dd-H_2O three times. The desired nanoparticles were obtained (10 mg) after centrifugation at 13 400 rpm for 20 min.

Analysis of Galactose Amount on TGal-PTX@Cy3-SiO$_2$NP and TGal@Cy3SiO$_2$NP. The anthrone method[51,52] was used to determine galactose loading on the nanoparticles. **TGal-PTX@Cy3SiO$_2$NP** and **TGal@Cy3SiO$_2$NP** were dispersed in deionized water (0.5 mL) in an ice bath. A freshly prepared 0.5% (w/w) solution of anthrone in sulfuric acid (1 mL) was slowly added to this solution. The resulting solution was gently mixed and heated to 100 °C for 10 min. The absorption of the solution was measured at 620 nm and compared to a standard curve to determine the concentration of sugar ligand on the nanoparticle surface. Figure S3 is the standard curve for galactose quantification.

Cell Culture. HepG2 cells were cultured in a 10 cm^2-dish with Dulbecco's Modified Eagle's Medium (DMEM, Gibco), 10% heat-inactivated fetal bovine serum (FBS, Gibco), 100 U/mL penicillin (Gibco), 100 μg/mL streptomycin (Gibco), and 0.25 μg/mL Fungizone (BioSOURCE). The cells were incubated at 37 °C in an ambient air/5% CO_2 atmosphere and subcultured every 3 days.

Observation of Internalized TGal-PTX@Cy3SiO$_2$NP, TGal@Cy3SiO$_2$NP, and PTX by Fluorescent Immunocytochemistry. HepG2 cells (2×10^4) were seeded onto sterile glass coverslips, placed in 24-well plates, and cultured in 1 mL DMEM medium containing 10% FBS overnight. **TGal-PTX@Cy3SiO$_2$NP** and **TGal@Cy3SiO$_2$ NP** (100 μg/mL in 0.5 mL serum-free DMEM) were sonicated for 15 min and then added to the HepG2 cultures. An equivalent concentration (5.3 μM, 0.5 mL) of the tubulin polymerization inhibitor PTX in serum-free DMEM with 3.3% DMSO was added to the HepG2 culture well, and the results were used as a positive control. After incubation at 37 °C for 2 days, LysoTracker Green DND-26 (Molecular Probes) was added to the wells (final concentration, 120 nM), and the cells were incubated for another 30 min. The cells were washed with 1 mL of serum-free DMEM three times and with 1% PEG-400 in PBS three times to remove the nanoparticles. The cell-seeded coverslips were fixed by immersion in 1 mL of 4% paraformaldehyde in PBS (w/v) at room temperature for 15 min. The cells were permeabilized with 1 mL of 0.1% Triton-X 100 in PBS (v/v) for 5 min at room temperature (rt) and washed with 1 mL of PBS. These procedures were repeated three times. The samples were blocked with 1 mL of 3% BSA (w/v) in PBS for 2 h at rt to avoid nonspecific binding. The mouse monoclonal tubulin antibody [DM1A + DM1B] (Abcam) was introduced to the blocking solution and incubated for another 2 h at rt. The samples were washed with 1 m L of PBST (0.5% Tween 20 (v/v) in PBS) three times, and 1 mL of the anti-mouse IgG DyLight 649 antibody (Jackson ImmunoResearch) diluted with 3% BSA (w/v) in PBS was introduced to the cell sample. The resulting mixture was incubated at rt for 1 h. After washing with 1 mL of PBST (0.5% Tween 20 (v/v) in PBS) three times, the samples were treated with 0.5 mL of 5 μg/mL 4,6-diamino-2-phenylindole (DAPI, Invitrogen) at rt for 15 min. Finally, the samples were mounted on Prolong antifade mounting medium (Invitrogen) and examined with a Zeiss LSM 710 confocal microscope (Carl Zeiss, GmbH).

Cytotoxicity Test of HepG2 Cell. HepG2 cells (1.2×10^4) were seeded in 100 μL DMEM containing 10% FBS in each well of a 96-well plate and allowed to attach for 24 h. All of the NP samples were sonicated for 15 min and then aliquot to the HepG2 cell culture wells. A series of concentrations (1.6, 3.2, 6.3, 12.5, and 25 μg/mL) of **TGal-PTX@Cy3SiO$_2$NP** or **TGal@Cy3SiO$_2$NP** in 100 μL serum-free DMEM was added to each well and incubated at 37 °C for 1 h. The wells were washed with PBS to remove the untaken NPs. The cells were cultured at 37 °C for 1 day. This process was repeated again and then the cells were cultured at 37 °C for another 2 days. Different concentrations of PTX drug (5.3, 2.7, 1.3, and 0.7 μM) in 100 μL serum-free DMEM with 1% DMSO were also added into cell culture well and the experimental procedures are almost the same as described in the NP treated experiment but with treatment of PTX for 3 h. To evaluate the cell toxicities of drugs, the WST-8 assay was performed. Per the manufacturer's instructions, the cells were washed with PBS and then treated with a WST-8 cell proliferation kit (Enzo Life Science). After incubation for 2 h, the formazan dye produced by the viable cells was measured at 450 nm using a SpectraMax M2^e microplate reader (Molecular Devices).

RESULTS AND DISCUSSION

We designed dialkyne **8** (Scheme 1) with the following considerations in mind: the two alkynes provide excellent selectivity and reactivity with azides as well as orthogonality toward each other.[38,39] Strain-promoted [3 + 2] azide−alkyne cycloaddition (SPAAC)[41−43] was envisioned to conjugate azido-functionalized PTX **12** (Scheme 2a). Subsequently, microwave-assisted Cu(I)-catalyzed [3 + 2] azide−alkyne cycloaddition (CuAAC) was used to immobilize T-Gal ligand **16** (Scheme 2b). Due to the length of the spacer units in dialkyne **8**, the T-Gal ligands are presented on the outside of the NP (Scheme 4). The presence of Gal at the external of NP should prevent the uptake of the NPs by macrophages, reduce the clearance by the RES,[14] and enhance the water solubility of the PTX-functionalized NP. Furthermore, this arrangement can trigger ligand−receptor interaction between the galactose molecules and the targeted ASGP-Rs on HepG2 cell surface.

Before proceeding with the synthesis of Cy3-doped silicon oxide NP loaded with PTX and T-Gal, solution-phase model studies were performed to investigate the feasibility and effectiveness of stepwise orthogonal click reaction on dialkyne **7**. As shown in Scheme 1, the (L)-lysine derivative **1** was chosen as a suitable scaffold to incorporate various alkynes for conjugation with the drug and ligand. Activation of the carboxylic acid group in **1** by using NHS and EDC was followed by coupling with monoalkyne **2** (for a detail synthesis of **2**, please see Supporting Information) to afford **3** with a 72% yield over two steps. After deprotection of Fmoc in **3**, the resulting product was reacted with the activated acid **4**[46] which is expected to link to the Cy3-silicon oxide NP to give **5**. Introduction of the second alkyne was achieved by deprotection of the Boc group of **5** and coupling with an activated cyclooctyne derivative **6**[42] to yield **7**, which was further deprotected to afford the dialkyne derivative **8** (total yield 32.4% over 7 steps from compound **1** to **8**). It is worth to note that cyclooctyne derivative would be decomposed in the relative harsh TFA contained conditions. Thus, to proceed dialkyne compound such as compound **7**, the harsh acidic

Scheme 3. Stepwise Synthesis of Compound 20 in the Solution Model Study[a]

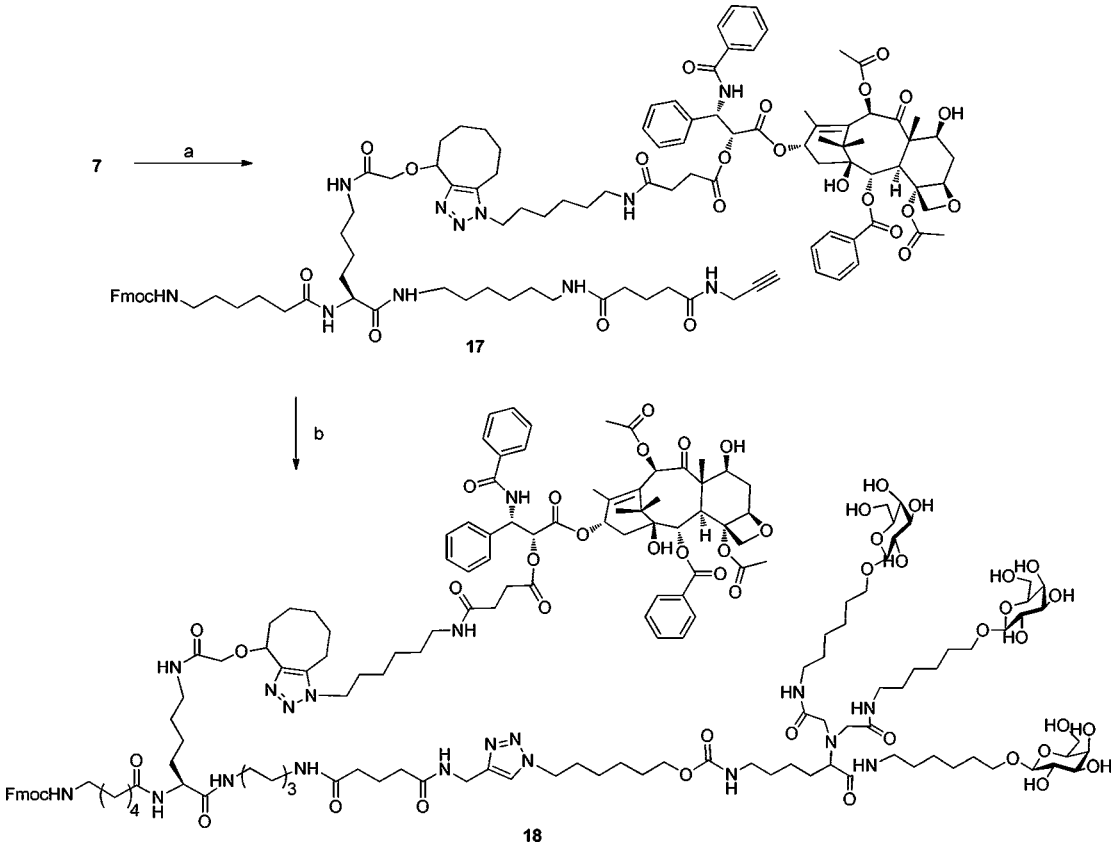

[a]Reagents and conditions: (a) **14**, DMF, rt, 6 h; (b) **18**, $CuSO_4{\cdot}5H_2O$, sodium ascorbate, THF/DMF/H_2O (5:1:1), 100 W, 0.5 h, quant.

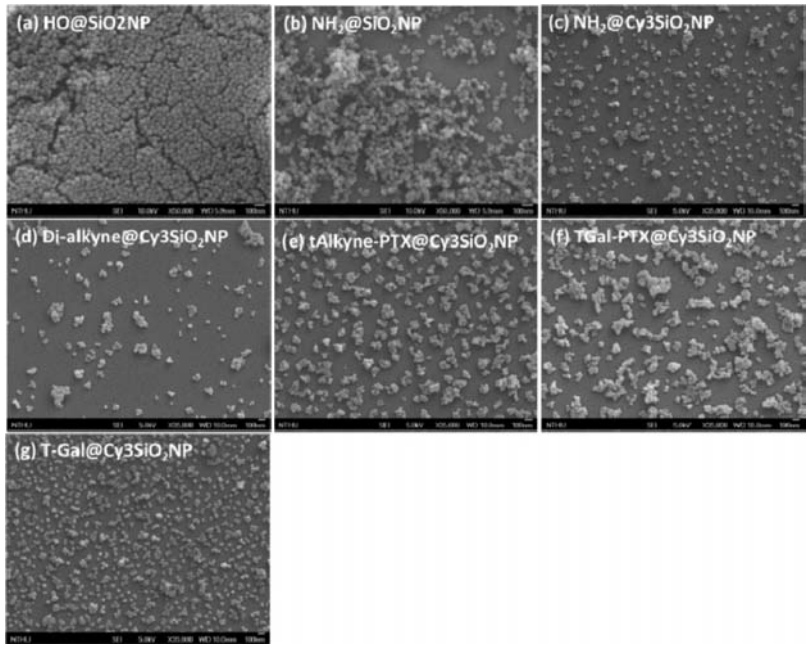

Figure 2. The SEM pictures of different silica oxide nanoparticles. (a) **HO@SiO_2NP** is shown a homosphere in a size around 40 nm. (b) **NH_2@SiO_2NP**, (c) **NH_2@Cy3SiO_2NP**, (d) **Dialkyne@Cy3SiO_2NP**, (e) **tAlkyne-PTX@Cy3SiO_2NP**, (f) **TGal-PTX@Cy3SiO_2NP**, and (g) **T-Gal@Cy3SiO_2NP** are all shown in a size around 50 nm. Scale bar: 100 nm.

conditions should be avoid when the cyclooctyne moiety is already in the part of structure.

With the required dialkyne in hand, we embarked upon the synthesis of azide-functionalized PTX and T-Gal to perform the click reactions. As shown in Scheme 2a, PTX **9** was converted to a 2′-*O*-succinyl-paclitaxel derivative using succinic anhydride **10**, and it was subsequently coupled with 6-azido hexanamine **11**[48] to yield the required azide-functionalized paclitaxel **12**

dx.doi.org/10.1021/bc400219t | *Bioconjugate Chem.* 2013, 24, 1698−1709

Scheme 4[a]

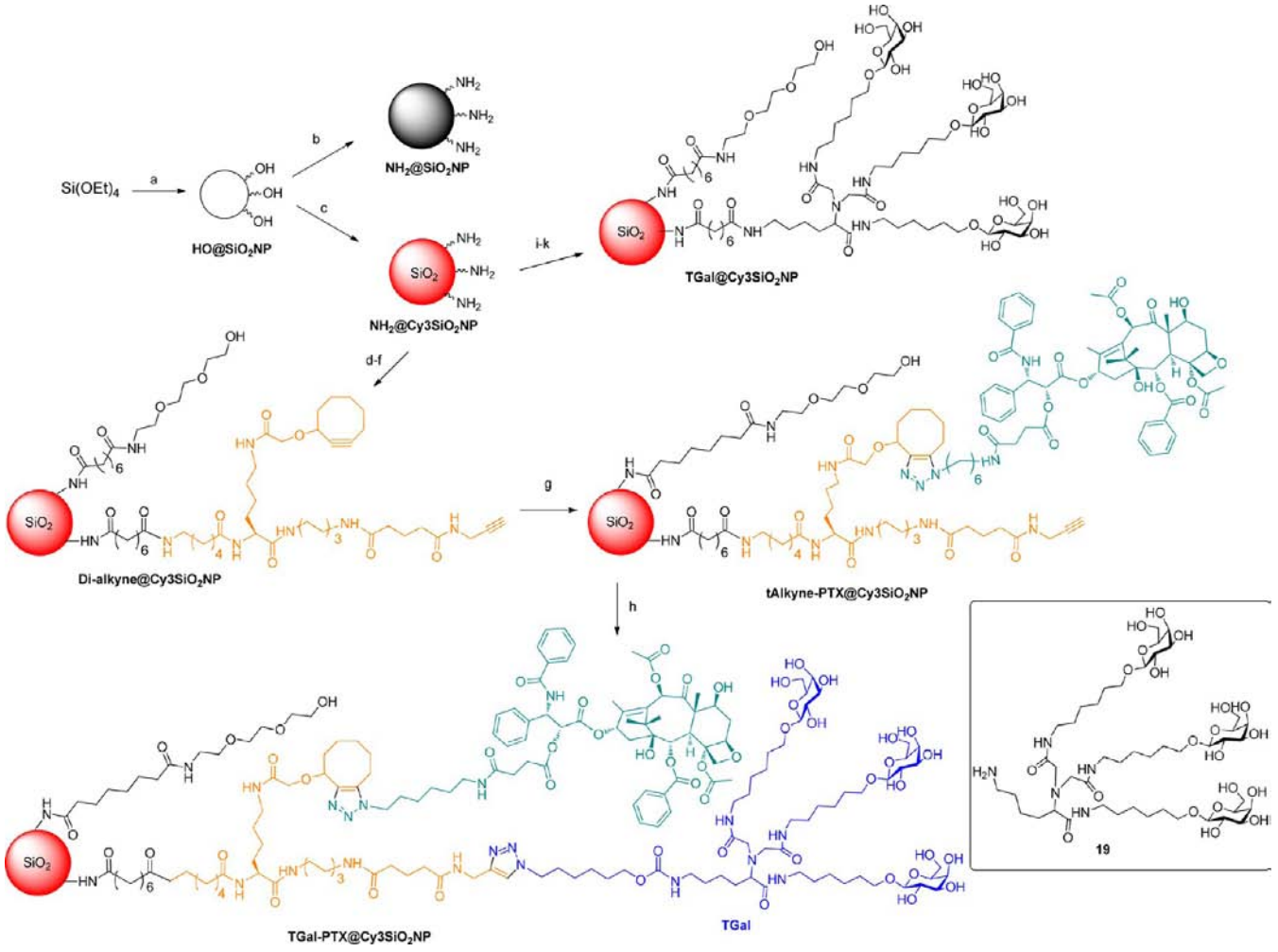

[a](a) NH_4OH, EtOH, rt, 12 h; (b) APS, dd-H_2O/PrOH, NH_4OH; (c) APS/Cy3-silane (100/1), dd-H_2O/PrOH, NH_4OH; (d) DSS, EDC, HOBT, NEt_3, DMSO, rt, 3 h; (e) **8**, EDC, HOBT, NEt_3, DMSO, rt, 18 h; (f) 50 mM amino-triethylene glycol, DMF, rt, 3 h; (g) **12**, DMF, 24 h; (h) **16**, sodium ascorbate, $CuSO_4$, THF/DMF/H_2O (5:1:1), 100 W, 75 °C, 1 h; (i) DSS, EDC, HOBT, NEt_3, DMSO, rt, 3 h; (j) **19**, EDC, HOBT, NEt_3, DMSO, rt, 18 h; (k) 50 mM amino-triethylene glycol, DMF, rt, 3 h.

(total yield 57.3% for 2 steps). Conjugation of *N*,*N*-bis[carboxymethyl]-L-lysine **13**[49] with 4-nitrophenyl carbonate-activated 6-azidohexan-1-ol **14**[26] in DMF/H_2O utilizing triethylamine gave the azide-functionalized lysine derivative, which was then coupled with galactosyl compound **15**[8] using HATU in DMF at 45 °C to furnish the azide-functionalized T-Gal derivative **16** (Scheme 2b, total yield 41.4% for 2 steps).

Having obtained the azide-functionalized PTX **12** and T-Gal ligand **16**, attention was focused on the ligation of these derivatives to check the efficiency of SOCC. As shown in Scheme 3, by taking advantage of the different reactivities of two alkynes, SPAAC-mediated click chemistry is expected to take place at cyclooctanyne, while CuAAC occurs at the terminal alkyne. The click reaction of PTX **12** with cyclooctanyne proceeded smoothly in DMF at room temperature for 6 h to give PTX-loaded **17** in quantitative yield. Then, microwave was applied to facilitate the Cu-mediated click reaction. Irradiating at 100 W for 30 min gave **18** in quantitative yield. The reaction can be performed without microwave assistance, but it requires longer reaction time and provides lower yield. Figure S1 shows stepwise NMR spectra of the synthesis of compound **18**; the fingerprints for PTX and T-Gal are clearly visible.

It has been reported that the optimal size for NP-mediated cellular internalization is 40 to 50 nm,[22] and the size of the NP required to reduce the rate of clearance by macrophages and provide better circulation time in the body[23] is 80 nm. Particles with longer circulation times are better able to target the site of interest, and they should be 100 nm or less in diameter with a hydrophilic surface. Thus, particle size of our designed silicon oxide nanocarrier is ~50 nm. As shown in Figure 2 and Scheme 4, unfunctionalized silicon oxide nanocarrier **HO@SiO_2NP** was first synthesized in a 40 nm size by controlling the ammonia concentration.[20,21] Briefly, the synthesis involves stirring tetraethylorthosilicate (TEOS), ethanol, dd-water, and NH_4OH solution at room temperature for 12 h.[20,21] The surface of the resulting 40 nm nanoparticle, **HO@SiO_2NP**, was transformed to give amino functionality via a sol−gel process using 3-amino-propyl trimethoxysilane (APS) to give 50 nm **NH_2@SiO_2NP**. The SEM images were shown of each step of synthetic silicon oxide NPs in Figure 2. Fluorescent silica NPs are known to show less aggregation and little dye leakage when compared to polymeric NPs which display wide utility in

dx.doi.org/10.1021/bc400219t | *Bioconjugate Chem.* 2013, 24, 1698−1709

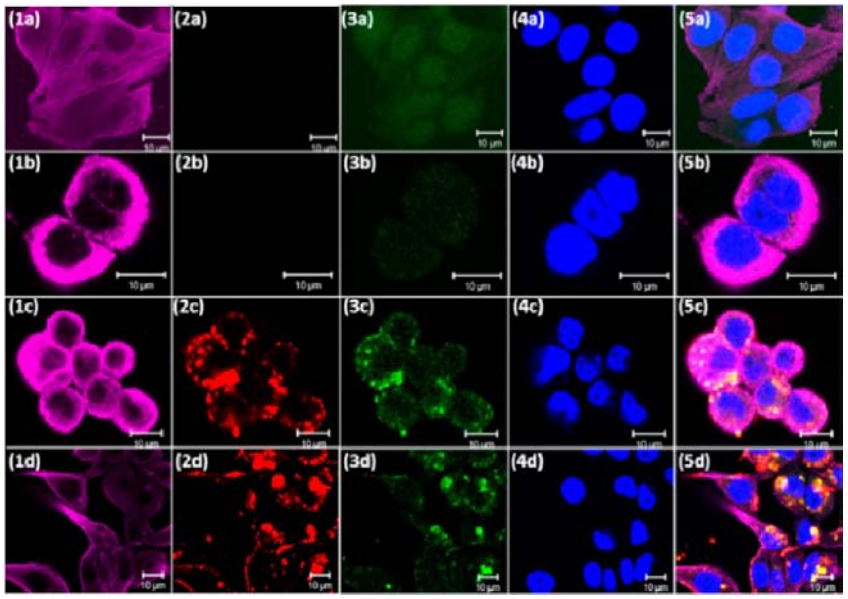

Figure 3. Confocal images of HepG2 cells treated with PTX (5.3 μM in 0.5 mL serum-free DMEM), **TGal-PTX@Cy3SiO$_2$NP** (100 μg/mL in 0.5 mL serum-free DMEM), or **TGal@Cy3SiO$_2$NP** (100 μg/mL in 0.5 mL serum-free DMEM) for 2 days. Each horizontal row of images (a-d) represents: (a) control without added reagents as control, (b) PTX with 3.3% DMSO as a positive control, (c) **TGal-PTX@Cy3SiO$_2$NP**, and (d) **TGal@Cy3SiO$_2$NP** as a negative control. The vertically arranged images (1−5) show: (1) purple color representing tubulin distribution; (2) red fluorescence arising from Cy3 dye on silicon oxide NP; (3) green fluorescence associated with LysoTracker Green DND-26 found within the endosomes and/or lysosomes; (4) cell nuclei stained with DAPI, which fluoresces blue; and (5) a merge of the images. The yellow fluorescence indicates that **TGal-PTX@Cy3SiO$_2$NP** and **TGal@Cy3SiO$_2$NP** colocalized with LysoTracker Green DND-26 in late endosomes and/or lysosomes. Scale bar: 10 μm.

bioanalysis and labeling.[53] Thus, the Cy3, a cyanine dye, was selected to be doped into NP due to its high fluorescence quantum yield and photostability.[54] To synthesize the fluorescent NPs, APS and Cy3-silane[50] were used in a 100:1 ratio in a sol−gel process to give **NH$_2$@Cy3SiO$_2$NP**. We found that, under these reaction conditions, the surface amine density and particle size of the NPs showed almost no change compared with **NH$_2$@SiO$_2$NP**. The competition method avoids self-quenching caused by tight packing of the dye on the NPs.[14,24] The amount of accessible amino groups on the surface of the dye-doped **NH$_2$@Cy3SiO$_2$NP** and the undoped **NH$_2$@SiO$_2$NP** was 236.2 ± 7.9 (~3.01 ± 0.10 NH$_2$/nm^2) and 250.5 ± 13.9 nmol/mg (~3.19 ± 0.17 NH$_2$/nm^2), respectively (Figure S2).

As shown in Scheme 4, the dialkyne compound **8** was conjugated with **NH$_2$@Cy3SiO$_2$NP** using suberic acid bis-*N*-hydroxysuccinimide ester (DSS) as a cross-linker and amino-triethylene glycol as a capping reagent to afford **Dialkyne@Cy3SiO$_2$NP**. Notably, a small amount of amine (5.3 ± 1.2 nmol/mg) on **Dialkyne@Cy3SiO$_2$NP** could be detected following the above procedure (Figure S2), indicating that the surface amine of **Dialkyne@Cy3SiO$_2$NP** was transformed to OSu. Taking advantage of the different reactivities of alkynes to azide as evidenced in the solution phase study, PTX was first introduced chemoselectively onto **Dialkyne@Cy3SiO$_2$NP** using an SPAAC reaction at the azido-functionalized PTX **12** in DMF. To ensure completion of the reaction, the reaction time was extended to 24 h. Excess costly PTX **12** was easily recovered by concentrating the reaction solution after removal of the NPs because the SPAAC step does not involve other reagent/catalyst. Then, the T-Gal ligand **16** was coupled with the PTX-loaded NP (**tAlkyne-PTX@Cy3SiO$_2$NP**) using microwave-assisted CuAAC for 1 h to yield **TGal-PTX@Cy3SiO$_2$NP**. Similar to the synthesis of the **Dialkyne@Cy3SiO$_2$NP**, control **TGal@Cy3SiO$_2$NP** was synthesized by reacting the T-Gal ligand **19**[8] with DSS-activated **NH$_2$@Cy3SiO$_2$NP** in the presence of EDC, HOBT, and NEt$_3$ in DMSO. The amount of galactose on **TGal-PTX@Cy3SiO$_2$NP** and **TGal@Cy3SiO$_2$NP** was determined by an Anthrone assay to be 157.89 ± 7.15 (2.04 ± 0.09 Gal/nm^2) and 32.29 ± 0.35 nmol/mg (0.42 ± 0.01 Gal/nm^2), respectively. The sugar amount differed from the silica NPs (obtained by amide bond formation or double click chemistry) indicate that the conjugation efficiency of less-polar trifunctional compound **8** with OSu-activated **NH$_2$@Cy3SiO$_2$NP** is higher than that of hydrophilic T-Gal ligand **19**. Although the conjugation yield between **8** and OSu-activated **NH$_2$@Cy3SiO$_2$NP** was only approximately 20% (estimated based on previous observations),[55] the results show that click chemistry provides better overall conjugation efficiency. The amount of PTX on **TGal-PTX@Cy3SiO$_2$NP** was estimated to be one-third of the amount of galactose ligand: 52.63 ± 7.15 nmol/mg (0.68 ± 0.09 PTX/nm^2).

To evaluate the anticancer activity of the synthesized NPs, HepG2 cells were seeded onto sterile glass coverslips and cultured in DMEM medium containing 10% FBS overnight. **TGal-PTX@Cy3SiO$_2$NP** and **TGal@Cy3SiO$_2$NP** (100 μg/mL in 0.5 mL serum-free DMEM) were sonicated for 15 min and added to the HepG2 cultures for 2 days. An equivalent concentration (5.3 μM) of free PTX was used as a positive control and incubated with HepG2 for 2 days. Confocal fluorescence microscopy image studies were performed (Figures 3 and S4−S7) to understand the fate and effect of NPs in the cell. In Figure 3, each horizontal row of images (a-d) represents: (a) control without added reagents, (b) PTX with 3.3% DMSO as a positive control, (c) **TGal-PTX@**

Cy3SiO$_2$NP, and (d) **TGal@Cy3SiO$_2$NP** as a negative control. Tubulin was labeled with mouse monoclonal tubulin antibody and visualized using an antimouse IgG DyLight 649 antibody to give the purple color shown in Figure 3 (1). The red fluorescence in Figure 3 (2) indicates the presence of Cy3 that has been incorporated into **TGal-PTX@Cy3SiO$_2$NP** and **TGal@Cy3SiO$_2$NP**. To locate **TGal-PTX@Cy3SiO$_2$NP** and **TGal@Cy3SiO$_2$NP** after endocytosis, LysoTracker Green DND-26 was used to label late endosomes and lysosomes (indicated as green color in Figure 3 (3)), whereas the nucleus was labeled with the blue fluorescent dye 4,6-diamino-2-phenylindole (DAPI), Figure 3 (4). The merged image (Figure 3 (5)) shows that late endosomes are yellow fluorescence due to colocalization of red fluorescence (**TGal-PTX@Cy3SiO$_2$NP** or **TGal@Cy3SiO$_2$NP**) and green fluorescence (LysoTracker Green DND-26). Therefore, the NPs accumulated in late endosomes and/or lysosomes after endocytosis. In our previous studies,[8] different ligands (such as galatoside, glucoside, and sialoside) were separately conjugated on a specifically designed Cy3-labeled magnetic nanoparticle (MNP), and their uptake by HepG2 was evaluated. The results showed that galatoside as surface ligand on MNP provides the best delivery efficiency. Besides, the galatoside modified MNP displays the specific targeting to HepG2 cell over HeLa cell, indicating the selective delivery through ASGP-R mediate endocytosis.[8] As shown in Figures 3 (2c) and (2d), the red color spreads throughout the cytoplasm, providing evidence that the NPs escaped from endosomes after receptor-mediated endocytosis. Because PTX is a microtubule-stabilizing agent, it promotes polymerization of tubulin, causing cell death by disrupting cell division.[56,57] As shown in Figure 3 row (1), the tubulin pattern of the **TGal-PTX@Cy3SiO$_2$NP**-treated cell (Figure 3 (1c)) is the similar as that of the PTX-treated cell (Figure 3 (1b)), indicating that the NPs were internalized into cells and PTX presented its fuction.[30,31,58] Notably, it has been reported that the paclitaxel of PTX prodrug can be released by esterase located in cytoplasma to execute microtubule inhibition and apoptosis once the prodrug is delivered into the cell.[30,33,35,36] By contrast, the confocal image of **TGal@Cy3SiO$_2$NP** (negative control, Figure 3 row (d)) showed the same uptake mechanism but without a change in cell morphology or tubulin pattern.

In order to evaluate the efficacy of **TGal-PTX@Cy3SiO$_2$NP**, the cell proliferation assay was performed. As shown in Figure 4, HepG2 cells were treated with a series of concentrations of **TGal-PTX@Cy3SiO$_2$NP** or **TGal@Cy3SiO$_2$NP** in serum-free DMEM for 1 h and then cultured for 1 day. After repeating this process for twice, the cells were then continuously cultured for another 2 days and the WST-8 assay was performed. The PTX concentration of **TGal-PTX@Cy3SiO$_2$NP** at 25, 12.5, 6.3, 3.2, and 1.6 μg/mL is approximately to 1.3, 0.7, 0.35, 0.17, and 0.09 μM based on the estimated PTX amount by one-third of the amount of galactose ligand on **TGal-PTX@Cy3SiO$_2$NP**. Furthermore, different concentrations of PTX drug (5.3, 2.7, 1.3, and 0.7 μM) in serum-free DMEM with 1% DMSO were also added into cell culture wells and the experiments, almost the same as described in the NP treated experiments but with treatment of 3 h, were performed (Figure 4b). The cell proliferation results revealed that the cytotoxicities of both **TGal-PTX@Cy3SiO$_2$NP** and PTX drug are dose-dependent and **TGal@Cy3SiO$_2$NP** is nontoxic. However, **TGal-PTX@Cy3SiO$_2$NP** showed 50% cell killing effect at the concentration of 12.5 μg/mL (corresponding to 0.7 μM of PTX) while, under the same concentration, free PTX drug shows no cytotoxicity

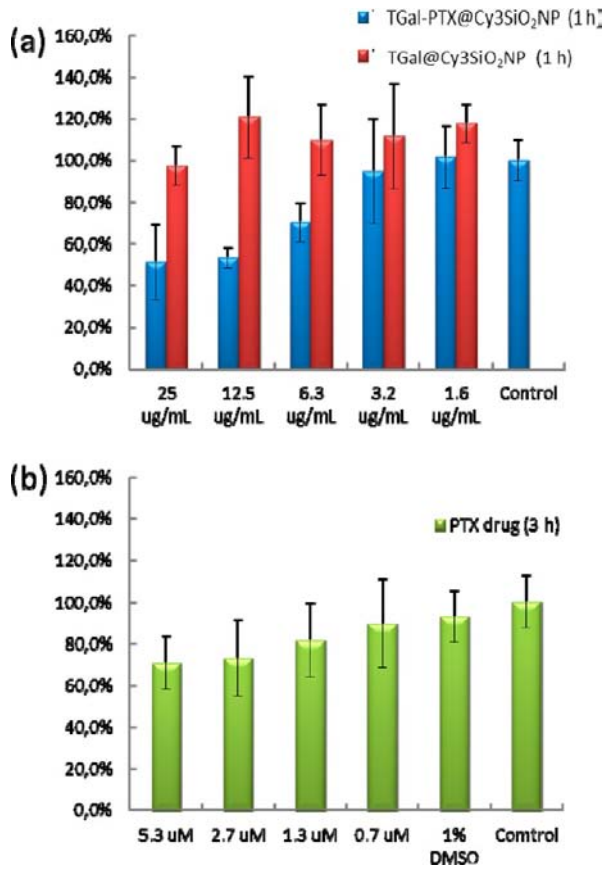

Figure 4. Cytotoxicities of (a) **TGal-PTX@Cy3SiO$_2$NP** and **TGal@Cy3SiO$_2$NP** and (b) PTX drug assessed using the WST-8 assay. The cells were treated with **TGal-PTX@Cy3SiO$_2$NP** and **TGal@Cy3SiO$_2$NP**, respectively, for 1 h or PTX for 3 h, and then incubated for 1 day at 37 °C. This process was repeated twice and then the cells were continuously cultured for another 2 days. The PTX concentration of **TGal-PTX@Cy3SiO$_2$NP** at concentration of 25, 12.5, 6.3, 3.2, and 1.6 μg/mL is approximately to 1.3, 0.7, 0.35, 0.17, and 0.09 μM.

(data is not showed) and the longer treatment (for 3 h) of it displays only very low toxicity on HepG2 cells. Although, for PTX sensitive cells such as the breast cancer cell, the effective cell killing concentration of PTX is around nM range, HepG2 cell was not sensitive to PTX drug.[59,60] The low toxicity of free PTX on HepG2 cell may be due to its slow and nonspecific diffusion rate to pass through cell membrane. Nevertheless, our designed **TGal-PTX@Cy3SiO$_2$NP** provides much higher cell killing effect than free PTX (Figure 4), indicating the advantage of specifically targeting. Moreover, it should be noted that 1% DMSO was required to solubilize free PTX in medium. The presence of DMSO may influence the cell life cycle and lead to cytotoxicity or allergic reaction.[44,45] Overall, the developed mutlifunctionalized NP was demonstrated as an attractive drug carrier for specific and efficient delivery of drug to the target cell.

■ CONCLUSIONS

In summary, the surface of the SiO$_2$ nanoparticles was functionalized with a trifunctional bridge linker with orthogonally clickable dialkyne **8**, which increases the surface availability for further functionalization by stepwise orthogonal click chemistry (SOCC). Because the SPAAC reaction does not

dx.doi.org/10.1021/bc400219t | Bioconjugate Chem. 2013, 24, 1698−1709

require other chemical reagents, the expensive PTX can be easily recovered. The use of a trivalent galactosyl ligand, which interacts with the ASGP-Rs on the surface of HepG2 cells, not only provides a targeting function, but also overcomes the inherent low water solubility of PTX. The *in vitro* assays indicate that **TGal-PTX@Cy3SiO$_2$NP** was trapped in the cell and escaped from endosomes. Due to the specific targeting of TGal moiety and receptor-mediated endocytosis, **TGal-PTX@Cy3SiO$_2$ NP** provides much better cell killing effect than that of free PTX at the same drug concentration, although HepG2 cell is not sensitive to PTX. Thus, it is anticipated that the **Dialkyne@Cy3SiO$_2$NP** could serve as an optimal nanocarrier for the specific delivery of anticancer drugs.

■ ASSOCIATED CONTENT

Ⓢ Supporting Information

Synthesis, analytical data and spectra. This material is available free of charge via the Internet at http://pubs.acs.org.

■ AUTHOR INFORMATION

Corresponding Author

*Tel: (+) 886-3-5753147. E-mail: cclin66@mx.nthu.edu.tw.

Notes

The authors declare no competing financial interest.

■ ACKNOWLEDGMENTS

This research was supported by National Science Council of Taiwan, National Tsing Hua University, and Academia Sinica, Taiwan. We thank Drs. I-Hui Chen and Hau-Shien Chan for helpful discussion, and Markus Weishaupt, Drs. L. Vijaya Raghava Reddy, and Dominea Rathwell for assisting the preparation of the manuscript.

■ REFERENCES

(1) Ferrari, M. (2005) Cancer nanotechnology: opportunities and challenges. *Nat. Rev. Cancer 5*, 161−171.
(2) Peer, D., Karp, J. M., Hong, S., Farokhzad, O. C., Margalit, R., and Langer, R. (2007) Nanocarriers as an emerging platform for cancer therapy. *Nat. Nanotechnol. 2*, 751−760.
(3) Davis, M. E., Chen, Z., and Shin, D. M. (2008) Nanoparticle therapeutics: an emerging treatment modality for cancer. *Nat. Rev. Drug Discovery 7*, 771−782.
(4) Doane, T. L., and Burda, C. (2012) The unique role of nanoparticles in nanomedicine: imaging, drug delivery and therapy. *Chem. Soc. Rev. 41*, 2885−2911.
(5) Xie, J., Lee, S., and Chen, X. (2010) Nanoparticle-based theranostic agents. *Adv. Drug Delivery Rev. 62*, 1064−1079.
(6) Lin, C. C., Yeh, Y. C., Yang, C. Y., Chen, C. L., Chen, G. F., Chen, C. C., and Wu, Y. C. (2002) Selective binding of mannose-encapsulated gold Nanoparticles to type 1 Pili in *Escherichia coli*. *J. Am. Chem. Soc. 124*, 3508−3509.
(7) Marradi, M., Chiodo, F., Garcia, I., and Penadés, S. (2013) Glyconanoparticles as multifunctional and multimodal carbohydrate systems. *Chem. Soc. Rev. 42*, 4728−4745.
(8) Lai, C.-H., Lin, C.-Y., Wu, H.-T., Chan, H.-S., Chuang, Y.-J., Chen, C.-T., and Lin, C.-C. (2010) Galactose encapsulated multi-functional nanoparticle for HepG2 cell internalization. *Adv. Funct. Mater. 20*, 3948−3958.
(9) Chien, W.-T., Yu, C.-C., Liang, C.-F., Lai, C.-H., Lin, P.-C., Lin, C.-C. (2011) Functionalized Glyconanoparticles for the Study of Glycobiology. In *Petite and Sweet: Glyco-Nanotechnology as a Bridge to New Medicines*, pp 15−36, Chapter 2, American Chemical Society.
(10) Montet, X., Funovics, M., Montet-Abou, K., Weissleder, R., and Josephson, L. (2006) Multivalent effects of RGD peptides obtained by nanoparticle display. *J. Med. Chem. 49*, 6087−6093.
(11) Hong, S., Leroueil, P., Majoros, I. J., Orr, B. G., Baker, J. R., and Holl, M. M. B. (2007) The binding avidity of a nanoparticle-based multivalent targeted drug delivery platform. *Chem. Biol. 14*, 107−115.
(12) Ruoslahti, E., Bhatia, S. N., and Sailor, M. J. (2010) Targeting of drugs and nanoparticles to tumors. *J. Cell Biol. 188*, 759−768.
(13) Hawkins, M. J., Soon-Shiong, P., and Desai, N. (2008) Protein nanoparticles as drug carriers in clinical medicine. *Adv. Drug Delivery Rev. 60*, 876−885.
(14) Adiseshaiah, P. P., Hall, J. B., and McNeil, S. E. (2010) Nanomaterial standards for efficacy and toxicity assessment. *Wiley Interdiscip. Rev. Nanomed. Nanobiotechnol. 2*, 99−112.
(15) van Blaaderen, A., and Vrij, A. (1992) Synthesis and characterization of colloidal dispersions of fluorescent, monodisperse silica spheres. *Langmuir 8*, 2921−2931.
(16) Ow, H., Larson, D. R., Srivastava, M., Baird, B. A., Webb, W. W., and Wiesner, U. (2005) Bright and stable core-shell fluorescent silica nanoparticles. *Nano Lett. 5*, 113−117.
(17) Kim, S. H., Jeyakumar, M., and Katzenellenbogen, J. A. (2007) Dual-Mode Fluorophore-Doped Nickel Nitrilotriacetic Acid-Modified Silica Nanoparticles Combine Histidine-Tagged Protein Purification with Site-Specific Fluorophore Labeling. *J. Am. Chem. Soc. 129*, 13254−13264.
(18) Yan, J., Estévez, M. C., Smith, J. E., Wang, K., He, X., Wang, Lin, and Tan, W. (2007) Dye-doped nanoparticles for bioanalysis. *Nano Today 2*, 44−50.
(19) Bae, S. W., Tan, W., and Hong, J.-I. (2012) Fluorescent dye-doped silica nanoparticles: new tools for bioapplications. *Chem. Commun. 48*, 2270−2282.
(20) Davies, G.-L., Barry, A., and Gun'ko, Y. K. (2009) Preparation and size optimization of silica nanoparticles using statistical analyses. *Chem. Phys. Lett. 468*, 239−244.
(21) Stöber, W., Fink, A., and Bohn, E. (1968) Controlled growth of monodisperse silica spheres in the micron size range. *J. Colloid Interface Sci. 26*, 62−69.
(22) Jiang, W., Kim, B. Y. S., Rutka, J. T., and Chan, W. C. W. (2008) Nanoparticle-mediated cellular response is size-dependent. *Nat. Nanotechnol. 3*, 145−150.
(23) Fang, C., Shi, B., Pei, Y. Y., Hong, M. H., Wu, J., and Chen, H. Z. (2006) In vivo tumor targeting of tumor necrosis factor-alpha-loaded stealth nanoparticles: effect of MePEG molecular weight and particle size. *Eur. J. Pharm. Sci. 27*, 27−36.
(24) Zhao, X., Bagwe, R. P., and Tan, W. (2004) Development of organic-dye-doped silica nanospheres in a reverse microemulsion. *Adv. Mater. 16*, 173−176.
(25) Dong, X., Mattingly, C. A., Tseng, M. T., Cho, M. J., Liu, Y., Adams, V. R., and Mumper, R. J. (2009) Doxorubicin and paclitaxel-loaded lipid-based nanoparticles overcome multidrug resistance by inhibiting P-glycoprotein and depleting ATP. *Cancer Res. 69*, 3918−3926.
(26) Lai, C.-H., Lin, Y.-C., Chou, F.-I., Liang, C.-F., Lin, E.-W., Chuang, Y.-J., and Lin, C.-C. (2012) Design of multivalent galactosyl carborane as a targeting specific agent for potential application to boron neutron capture therapy. *Chem. Commun. 48*, 612−614.
(27) Gibson, J. D., Khanal, B. P., and Zubarev, E. R. (2007) Paclitaxel-functionalized gold nanoparticles. *J. Am. Chem. Soc. 129*, 11653−11661.
(28) Hwu, J. R., Lin, Y. S., Josephrajan, T., Hsu, M.-H., Cheng, F.-Y., Yeh, C.-S., Su, W.-C., and Shieh, D.-B. (2008) Targeted paclitaxel by conjugation to iron oxide and gold nanoparticles. *J. Am. Chem. Soc. 131*, 66−68.
(29) Chen, J., Chen, S., Zhao, X., Kuznetsova, L. V., Wong, S. S., and Ojima, I. (2008) functionalized single-walled carbon nanotubes as rationally designed vehicles for tumor-targeted drug delivery. *J. Am. Chem. Soc. 130*, 16778−16785.
(30) Liu, K. K., Zheng, W. W., Wang, C. C., Chiu, Y. C., Cheng, C. L., Lo, Y. S., Chen, C., and Chao, J. I. (2010) Covalent linkage of nanodiamond-paclitaxel for drug delivery and cancer therapy. *Nanotechnology 21*, 315106.

(31) Chorny, M., Fishbein, I., Yellen, B. B., Alferiev, I. S., Bakay, M., Ganta, S., Adamo, R., Amiji, M., Friedman, G., and Levy, R. J. (2010) Targeting stents with local delivery of paclitaxel-loaded magnetic nanoparticles using uniform fields. *Proc. Natl. Acad. Sci. U.S.A. 107*, 8346−8351.
(32) Wang, Y., Wang, Y., Xiang, J., and Yao, K. (2010) Target-specific cellular uptake of taxol-loaded heparin-PEG-folate nanoparticles. *Biomacromolecules 11*, 3531−3538.
(33) Zhang, X.-Q., Xu, X., Lam, R., Giljohann, D., Ho, D., and Mirkin, C. A. (2011) A strategy for increasing drug solubility and efficacy through covalent attachment to polyvalent DNA-nanoparticle conjugates. *ACS Nano 5*, 6962−6970.
(34) Mo, R., Jin, X., Li, N., Ju, C., Sun, M., Zhang, C., and Ping, Q. (2011) The mechanism of enhancement on oral absorption of paclitaxel by N-octyl-O-sulfate chitosan micelles. *Biomaterials 32*, 4609−4620.
(35) Das, M., Bandyopadhyay, D., Mishra, D., Datir, S., Dhak, P., Jain, S., Maiti, T. K., Basak, A., and Pramanik, P. (2011) "Clickable", trifunctional magnetite nanoparticles and their chemoselective biofunctionalization. *Bioconjugate Chem. 22*, 1181−1193.
(36) Shan, L., Cui, S., Du, C., Wan, S., Qian, Z., Achilefu, S., and Gu, Y. (2012) A paclitaxel-conjugated adenovirus vector for targeted drug delivery for tumor therapy. *Biomaterials 33*, 146−162.
(37) Medarova, Z., Pham, W., Farrar, C., Petkova, V., and Moore, A. (2007) In vivo imaging of siRNA delivery and silencing in tumors. *Nat. Med. 13*, 372−377.
(38) Lim, R. K. V., and Lin, Q. (2010) Bioorthogonal chemistry: recent progress and future directions. *Chem. Commun. 46*, 1589−1600.
(39) Kele, P., Mezo, G., Achatz, D., and Wolfbeis, O. S. (2009) Dual labeling of biomolecules by using click chemistry: a sequential approach. *Angew. Chem., Int. Ed. 48*, 344−347.
(40) Achatz, D. E., Mezo, G., Kele, P., and Wolfbeis, O. S. (2009) Probing the activity of matrix metalloproteinase II with a sequentially click-labeled silica nanoparticle FRET probe. *ChemBioChem 10*, 2316−2320.
(41) Agard, N. J., Prescher, J. A., and Bertozzi, C. R. (2004) A strain-promoted [3 + 2] azide−alkyne cycloaddition for covalent modification of biomolecules in living systems. *J. Am. Chem. Soc. 126*, 15046−15047.
(42) Agard, N. J., Baskin, J. M., Prescher, J. A., Lo, A., and Bertozzi, C. R. (2006) A comparative Study of bioorthogonal reactions with azides. *ACS Chem. Biol. 1*, 644−648.
(43) Jewett, J. C., and Bertozzi, C. R. (2010) Cu-free click cycloaddition reactions in chemical biology. *Chem. Soc. Rev. 39*, 1272−1279.
(44) Damascelli, B., Cantu, G., Mattavelli, F., Tamplenizza, P., Bidoli, P., Leo, E., Dosio, F., Cerrotta, A. M., Di Tolla, G., Frigerio, L. F., Garbagnati, F., Lanocita, R., Marchiano, A., Patelli, G., Spreafico, C., Ticha, V., Vespro, V., and Zunino, F. (2001) Intraarterial chemotherapy with polyoxyethylated castor oil free paclitaxel, incorporated in albumin nanoparticles (ABI-007): Phase II study of patients with squamous cell carcinoma of the head and neck and anal canal: preliminary evidence of clinical activity. *Cancer 92*, 2592−2602.
(45) Griset, A. P., Walpole, J., Liu, R., Gaffey, A., Colson, Y. L., and Grinstaff, M. W. (2009) Expansile nanoparticles: synthesis, characterization, and in vivo efficacy of an acid-responsive polymeric drug delivery system. *J. Am. Chem. Soc. 131*, 2469−2471.
(46) Sundararajan, C., Besanger, T. R., Labiris, R., Guenther, K. J., Strack, T., Garafalo, R., Kawabata, T. T., Finco-Kent, D., Zubieta, J., Babich, J. W., and Valliant, J. F. (2010) Synthesis and characterization of rhenium and technetium-99m labeled insulin. *J. Med. Chem. 53*, 2612−2621.
(47) Cavallaro, G., Licciardi, M., Caliceti, P., Salmaso, S., and Giammona, G. (2004) Synthesis, physico-chemical and biological characterization of a paclitaxel macromolecular prodrug. *Eur. J. Pharm. Biopharm. 58*, 151−159.
(48) Kuzmin, A., Poloukhtine, A., Wolfert, M. A., and Popik, V. V. (2010) Surface functionalization using catalyst-free azide-alkyne cycloaddition. *Bioconjugate Chem. 21*, 2076−2085.
(49) Schmitt, L., Dietrich, C., and Tampe, R. (1994) Synthesis and characterization of chelator-lipids for reversible immobilization of engineered proteins at self-assembled lipid interfaces. *J. Am. Chem. Soc. 116*, 8485−8491.
(50) Chen, G., Song, F., Wang, X., Sun, S., Fan, J., and Peng, X. (2012) Bright and stable Cy3-encapsulated fluorescent silica nanoparticles with a large Stokes shift. *Dyes Pigm. 93*, 1532−1537.
(51) Koehler, L. H. (1952) Differentiation of carbohydrates by anthrone reaction rate and color intensity. *Anal. Chem. 24*, 1576−1579.
(52) Chien, Y. Y., Jan, M. D., Adak, A. K., Tzeng, H. C., Lin, Y. P., Chen, Y. J., Wang, K. T., Chen, C. T., Chen, C. C., and Lin, C. C. (2008) Globotriose-functionalized gold nanoparticles as multivalent probes for Shiga-like toxin. *ChemBioChem 9*, 1100−1109.
(53) Tan, W., Wang, K., He, X., Zhao, X. J., Drake, T., Wang, L., and Bagwe, R. P. (2004) Bionanotechnology based on silica nanoparticles. *Med. Res. Rev. 24*, 612−638.
(54) Wessendorf, M. W., and Brelje, T. C. (1992) Which fluorophore is brightest? A comparison of the staining obtained using fluorescein, tetramethylrhodamine, lissamine rhodamine, Texas red, and cyanine 3.18. *Histochemistry 98*, 81−85.
(55) Yu, C.-C., Kuo, Y.-Y., Liang, C.-F., Chien, W.-T., Wu, H.-T., Chang, T.-C., Jan, F.-D., and Lin, C.-C. (2012) Site-specific immobilization of enzymes on magnetic nanoparticles and their use in organic synthesis. *Bioconjugate Chem. 23*, 714−724.
(56) Schiff, P. B., and Horwitz, S. B. (1980) Taxol stabilizes microtubules in mouse fibroblast cells. *Proc. Natl. Acad. Sci. U.S.A. 77*, 1561−1565.
(57) Kavallaris, M. (2010) Microtubules and resistance to tubulin-binding agents. *Nat. Rev. Cancer 10*, 194−204.
(58) Lin, Y. S., Tungpradit, R., Sinchaikul, S., An, F. M., Liu, D. Z., Phutrakul, S., and Chen, S. T. (2008) Targeting the delivery of glycan-based paclitaxel prodrugs to cancer cells via glucose transporters. *J. Med. Chem. 51*, 7428−7441.
(59) McAuliffe, G., Roberts, L., and Roberts, S. (2002) Paclitaxel administration and its effects on clinically relevant human cancer and non cancer cell lines. *Biotechnol. Lett. 24*, 959−964.
(60) Gagandeep, S., Novikoff, P. M., Ott, M., and Gupta, S. (1999) Paclitaxel shows cytotoxic activity in human hepatocellular carcinoma cell lines. *Cancer Lett. 136*, 109−118.